RESEARCH

Open Access

Experimental and Analytical Studies for the Size Effect on the Axial Strength of High-Strength Concrete Walls with Various Fire-Damaged Areas

Yeonju Chun, Eunmi Ryu, Yeokyeong Lee, Heesun Kim[*] and Yeongsoo Shin[*]

Abstract

The purpose of this study is to investigate the effect of fire-damaged areas associated with wall width on the axial strength of fire-damaged reinforced concrete (RC) walls. Toward that goal, Finite Element (FE) models of RC walls in real scale are generated with various wall widths of (600, 1500, and 3000) mm and number of heated surfaces such as half-surface, single-surface and double-surfaces. For the analyses, experiments are used to obtain temperature distributions inside the walls depending on the fire-damaged areas, and to validate the FE models. The analytical results show that the axial strength of the fire-damaged wall increases linearly with the wall width, except that the ratios of axial force to wall width showed slightly off from the average for the case of walls heated on half of the surface. Using the axial strength data of fire-damaged concrete walls obtained from the current and previous studies, regression analysis is conducted to estimate axial strength reduction ratios of fire-damaged concrete walls, considering various influencing parameters, such as concrete strength, fire-damaged areas, wall width and height. As a conclusion, multiple linear regression formulations from the regressions analyses are able to estimate axial strength reduction ratios of the fire-damaged concrete walls considering various influencing parameters of the wall size, concrete strength and fire-damaged area and the estimations showed good agreements with the data collected from experiments and FE analyses.

Keywords: reinforced concrete wall, fire, fire-damaged area, wall width, regression analysis

1 Introduction

High-strength reinforced concrete walls (RC) having compressive strength over 40 MPa (Standard & Center: Design standard for high strength concrete, 2020) are widely used as core walls or partitioning walls in high-rise residential buildings in Korea. One of the special features of the fire-damaged wall is that the only partial surface of the wall can be exposed to fire depending on

architectural plan and fire incident. In this case, cross-sectional properties of the wall cannot be symmetric, leading to asymmetric deformations of the fire-damaged walls (Liu et al., 2010; Ngo et al., 2013; Nguyen et al., 2018). Moreover, it has been known that high-strength concrete has high thermal conductivity compared to normal strength concrete, which leads to significant degradation of structural performance when damaged by fire (Kodur & Sultan, 1998).

One of the common issues regarding structure behaviors of fire-damaged wall where exposed to high temperatures enough to influence on strength of concrete has been about the effect of wall thickness on thermal and structural behavior. Kang et al. (Kang et al., 2016)

*Correspondence: hskim3@ewha.ac.kr; shinys@ewha.ac.kr
Department of Architectural and Urban Systems Engineering, Ewha Womans University, 52, Ewhayeodae-gil, Seodaemun-gu, Seoul, Republic of Korea

Chun *et al. Int J Concr Struct Mater*   (2022) 16:32

Page 2 of 14

experimentally and numerically studied the thermal behavior of walls having different thickness exposed to fire. Their study found that a relatively thick wall formed a moisture clog zone inside the wall, and prevented temperature being transferred from heated surface to the opposite side.

Researches with analytical methods have been developed to evaluate structural behaviors of fire-damaged RC structures (Lee & Lee, 2013; O'Meagher & Bennetts, 1991). With analytical methods, a computer-based model for investigating behavior of fire-damaged RC walls was introduced in early days as 1990s (O'Meagher & Bennetts, 1991). The model was based on strain compatibility in the wall and allowed to consider influencing parameters such as height-to-thickness ratio, cover thickness, and restraints. Lee and Lee predict the fire resistance of concrete walls having various height-to-thickness ratios, concrete strengths. In their study, it was found that the axial load levels of walls subjected to all-sided fire exposure were lower than one-sided fire exposure only (Lee & Lee, 2013). The predicted fire resistance were then compared with those obtained from existing code provisions such as ACI 216R-89 (ACI & TMS Committee216, 1989), AS3600 (AS3600, 2001), NZS3101 (NZS3101, 1995), and Eurocode 2 (Eurocode2, 2004), and showed good agreements. There have been studies using finite element (FE) models for predicting behaviors of fire-damaged walls with numerical methods(Kang et al., 2019; Ni & Bairely, 2018; Otmani-Benmehidi et al., 2014). Kang et al. also used FE modeling methods to investigate the effects of wall thickness and axial loading on the load-bearing capacity of fire-damaged RC walls. It was interesting to note that the axial loading during the fire tests did not affect on wall strength, while sensitivity of wall thickness to load-bearing capacity of the fire-damaged wall was significant in the walls with high slenderness ratio (Kang et al., 2019).

As mentioned earlier, the researches about fire-damaged walls have been focused more on the effect of wall height and thickness on structural behaviors of fire-damaged walls. Considering that wall width and fire-damaged area varies in wide range depending on the building plan, it is important to examine the effect of wall width in combination with the fire-damaged area on the strength of the fire-damaged wall. As a similar objects, previously Ryu et al. studied the effect of heated areas on the axial strength of the fire-damaged walls in small scale (Ryu et al., 2020). From the study, it was found that the axial strength of the wall heated on single-surface was degraded as much as the wall heated on double-surfaces, due to asymmetric behaviors of the wall heated on single-surface. However, the effects on wall width associated with fire-damaged areas on the strength of fire-damaged walls in real scale have not been studied even in the previous studies.
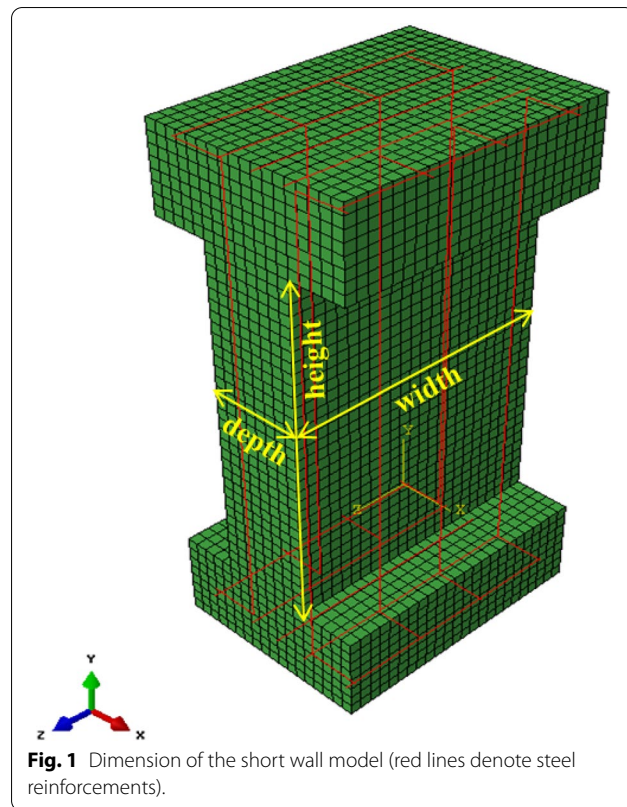
Therefore, this study aims to investigate the axial strength of fire-damaged RC walls having diverse wall width and fire-damaged area using analytical and statistical methods. Toward the goal, analytical studies using finite element (FE) models are conducted to predict axial strengths of fire-damaged RC walls with varied fire-damaged areas. The modeling methods are validated with the available experimental data and then applied to show the effect of wall lengths and fire-damaged areas on the axial strength of fire-damaged walls with high slenderness ratio. At last, multiple linear regression analyses are performed to estimate the axial strength of fire-damaged walls, which allows estimating strength reduction ratios of fire-damaged walls considering varied concrete strengths, wall dimensions, and fire-damaged areas.

2 Analytical Modeling Approach
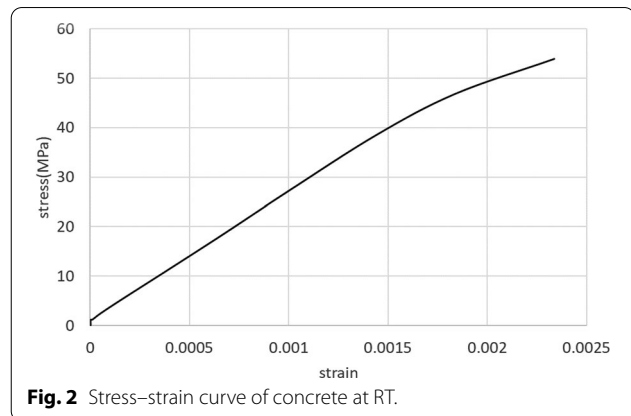### 2.1 Variables and the FE Models
FE model generation and structural analyses are conducted using commercial software Abaqus version 6.10-3 (Dassault Systems, Velizy-Villacoublay, France), using 3D continuum brick with reduced integration point (C3D8R) and 3D truss elements (T3D2) for concrete and steel reinforcements, respectively. Concrete and steels are assumed perfectly bonded because there were stirrups confining steel reinforcements and spalling of high-strength concrete was prevented in advance due to addition of polypropylene fiber in experiments.

The dimensions and variables are determined to be the same as those in the existing experimental data, as shown in Fig. 1 and Table 1. Temperature information of the inside the wall heated with ISO-834 standard heating curve from previously conducted experiments (Chun, 2019; Chun et al., 2018; Kang et al., 2019). Effect of temperature distributions on strength of the wall was included in the analysis by implementing temperature-dependent stress–strain curves of concrete in the corresponding section of the wall as shown in Fig. 4. The model included perfect bond between the concrete and the reinforcing steel bars during the analysis, because (1) vertical steel bars were confined by the lateral bars with enough anchorage length, and (2) there was no de-bonding of steel bars observed from the experiments. In addition, failure was determined when numerical instability occurs due to material and geometrical non-linearity. As the concrete develops plasticity and wall deformation increases, numerical instability occurs, which leads to termination of analysis after reasonable number of time increment control for convergence. In the ABAQUS, the time increment was increased by 50% in default if the analyses were converged in the

Chun *et al. Int J Concr Struct Mater*   (2022) 16:32

Page 3 of 14

Fig. 1 Dimension of the short wall model (red lines denote steel reinforcements).

Fig. 2 Stress–strain curve of concrete at RT.

Table 2 Strength and elastic modulus for concrete and steel.

Concrete		Steel	
28-day compressive strength (MPa)	Elastic modulus (GPa)	Yield strength (MPa)	Tensile strength (MPa)
53.9	26.7	538	623

Table 3 Reduction ratio of strength and elastic modulus of concrete due to heat (adopted Cheng et al. (Cheng et al., 2004)).

Temperature (°C)	Reduction ratio of concrete strength	Reduction ratio of elastic modulus of concrete
20	0	0
100	0.244	0.229
200	0.245	0.408
300	0.247	0.530
400	0.252	0.649
500	0.262	0.745
600	0.551	0.842
700	0.685	0.904
800	0.853	0.973
900	0.955	0.985

Table 1 Variables of the FE model.

FE model	Wall sizes	Heated exposure surface
54S_CL	600 mm (width) 1,200 mm (height) 200 mm (thickness)	None
54S_1H		Half-surface
54S_1F		Single-surface
54S_2F		Double-surfaces

two successive increments and decreased by 25% if the analyses were diverged or not converged within 16 iterations (ABAQUS, 2010). For effective calculation, maximum and minimum time increments were set as 100 s and 1×10^{-5} sec, respectively. The bottom surface of the model is fixed in all translational directions, while the top head of the wall is restrained in the horizontal direction only for vertical loading prescription. The analysis considers both material and geometrical nonlinearity. The material properties of the concrete at room temperature (RT) are obtained from the material strength tests as shown in Fig. 2 and Table 2, then the temperature-dependent material properties of the concrete are obtained according to the reduction ratios of elastic modulus and strength which are from 100 to 900 °C shown in Table 3. Both reduction ratios

of concrete strength and elastic modulus of concrete were adopted from the existing literatures (Cheng et al., 2004, Poon et al. 2001, Poon et al. 2016). From one of the literature, the authors were able to obtain reduction ratios of strength and elasticity per every 100 °C of temperature increase, while the temperature differences between the sections inside the wall model were prescribed with the temperatures smoothly changing from 100 to 900 °C. Therefore, reduction ratios at temperature levels not provided from the literatures (i.e., 150, 250, 350, 650, and 750 °C) were generated by conducting linear interpolation, i.e., reduction

Chun *et al. Int J Concr Struct Mater*   (2022) 16:32

Page 4 of 14

ratios at 150 °C was calculated as averaged ones of 10 and 200 °C. In addition, stress–strain curves of fire-damaged and non-damaged steel bars with diameter of 10 mm are obtained as Fig. 3 from the tensile strength tests, which are assigned to the steel elements in heated and unheated side of the walls, respectively. Damaged steel means reinforcing steel bars located near to the wall surface exposed to fire. Because the steel bars located far away from the fire were exposed to temperatures around 100 °C which was not enough to have influence on mechanical behaviors of steel bars, those were grouped as undamaged steel bars and the material properties measured at room temperature were implemented. Likewise, those located to the wall surface exposed to fire were grouped as damaged steel bars and degraded material properties obtained from the tests were used. Considering that the temperature difference at around damaged steel bars were minimal such as 400–650 °C, single level of material properties shown in Fig. 3 was used. The material properties of the concrete at various temperatures are assigned to the corresponding part of the FE model, considering temperature distributions through the wall thickness obtained from the experiments (Chun, 2019; Chun et al., 2018; Kang et al., 2019) and assigned temperatures are shown in Fig. 4.

2.2 Model Validation

In this section, the experimental method and results are briefly introduced to show overall tendencies of axial strength reduction due to fire and to validate the analytical models. More specific details of the experiment can be found in the previously published papers (Chun, 2019; Chun et al., 2018; Kang et al., 2019).
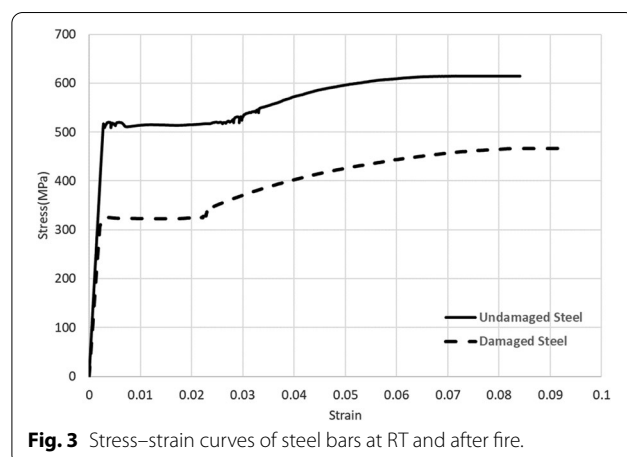
2.2.1 Experimental Program and the Results

Fig. 5a, b shows details of the wall specimens and locations of thermocouples. In order to measure temperature

Fig. 3 Stress–strain curves of steel bars at RT and after fire.
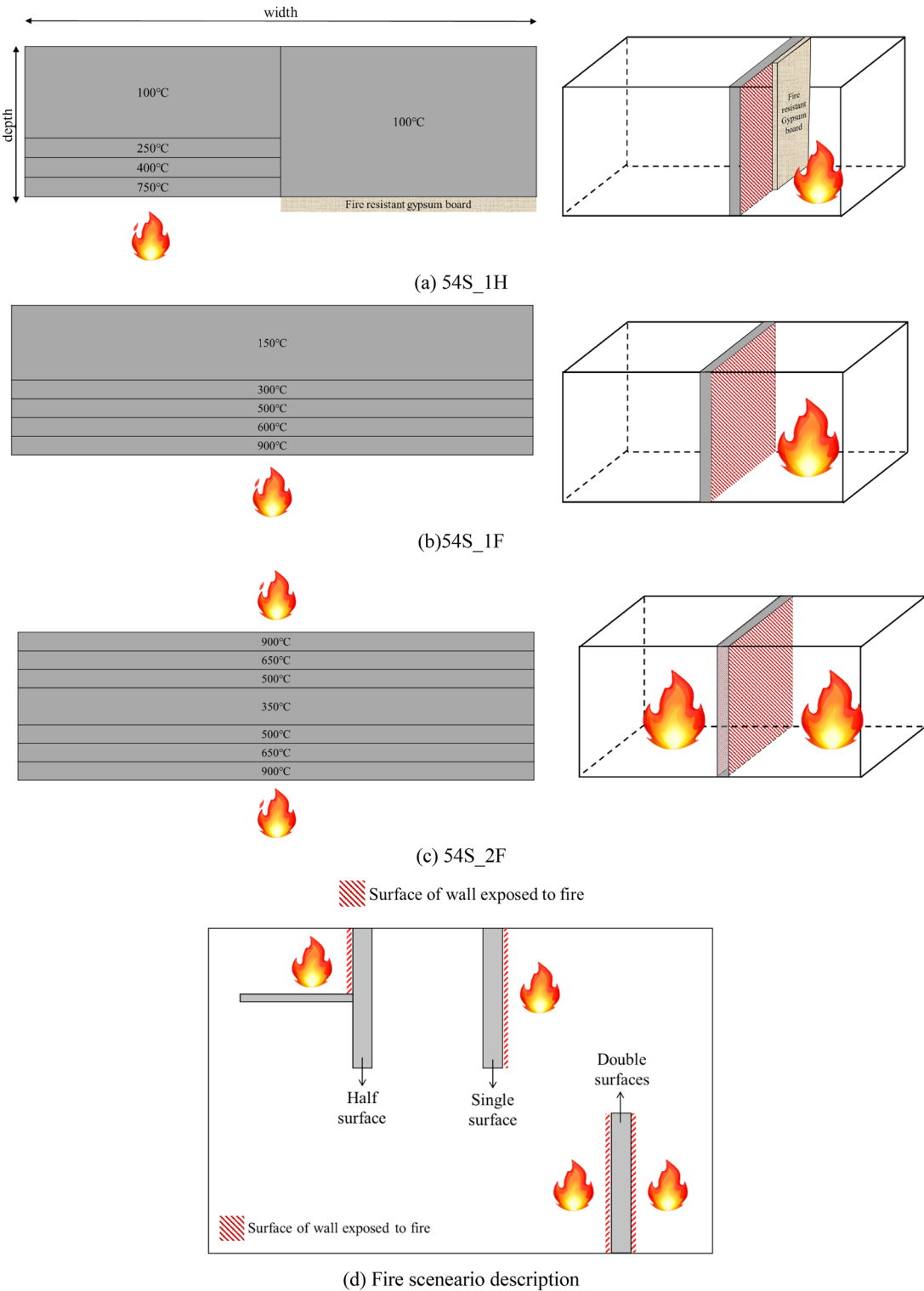
distributions during the fire tests, two groups of three thermocouples are located at C and D (Fig. 5a); the location of C is at mid-height of the wall, while location D is at mid-width of the wall. In each location, thermocouples are placed at 20, 40, and 100 mm from the heated surface, as illustrated in Fig. 5b. The concrete mix proportions are designed as shown in Table 4 to have target the 28 day strength of 60 MPa. In order to prevent spalling of high-strength concrete during heating, polypropylene (PP) fiber, which accounts for 0.15% of the total volume, are added to the concrete mixture

After 90 days of concrete curing, the wall specimens are heated for 2 h according to the ISO-834 standard heating curve inside the fire furnace, as shown in Fig. 6a. For the cases of half-surface and single-surface heated specimens, insulation is used to cover unheated areas. The fire-damaged wall specimens are then axially loaded until failure, and displacements are measured from 2 LVDTs placed on the front and back sides of the walls, as shown in Fig. 6b. Fig. 7 shows the meaning of the tested specimen names.

At the end of fire tests, the temperature distributions of the walls measured through the depth of the two different locations from the front view, C and D, shown in Fig. 5a and c are obtained as listed in Table 5. Generally, the temperatures at location C are obtained as the maximum temperature of the heated specimens. However, in the case of 54S_1H, the temperatures at the location D are presented in the table, because the thermocouples at location C give false values due to technical problems. As seen from the table, the maximum temperatures are around 419–820 °C at 20 mm depth from the heated surface, which may reduce strength of concrete more than 65%. Even at the middle-of-wall depth, reduction ratio of concrete strength is inferred as 23–31%, because the temperatures are in the range 117–247 °C. Regarding the heated area, the single-surface heated wall has the highest maximum temperature at 20 mm depth, while the half-surface heated wall has lowest maximum temperature at the same depth. In addition, it is interesting to note that the single-surface heated wall shows the higher maximum temperature at 20 mm depth and lower minimum temperature at the middle-of-wall than the double-surfaces heated wall. Table 6 shows the axial strength of fire-damaged walls, and reveals that the axial strength decreases due to fire by approximately 19.5–37.6%, compared to that of the control wall. Even though, in general, the reduction ratio increases with the heated area, the relationship between the heated area and the reduction ratio of axial strength is not linear. Compared to the half-surface heated wall, the axial strength of the single-surface heated wall is reduced significantly so that the reduction ratios of single-surface heated and the double-surfaces heated walls are almost same.
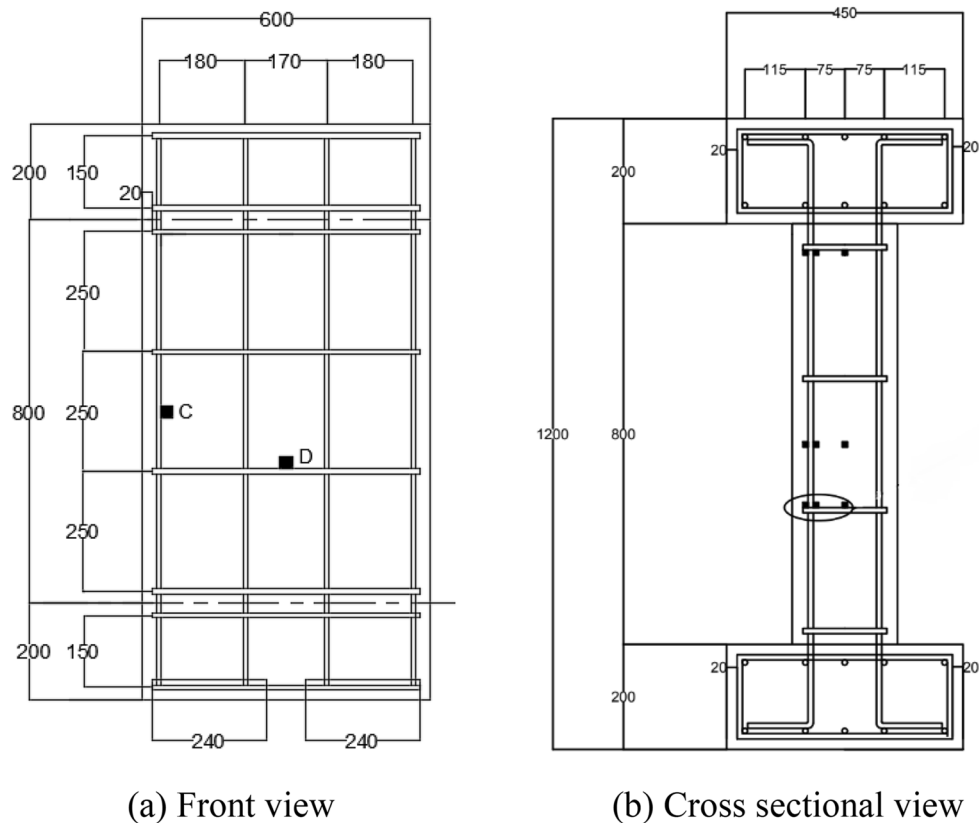
Chun *et al. Int J Concr Struct Mater*   (2022) 16:32

Page 5 of 14

Fig. 4 Temperature distribution (cross-sectional view) and corresponding fire scenario description.

Chun *et al. Int J Concr Struct Mater*   *(2022) 16:32*

Page 6 of 14

(a) Front view   (b) Cross sectional view

Fig. 5 Specimen details and locations of thermocouples (unit: mm).

Table 4 Mix proportion of concrete.

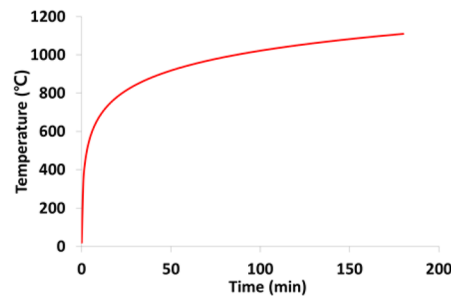| Target strength (MPa)	Water-to-cement ratio (%)	Cement (kg/m³)	Water	Fine aggregate	Coarse aggregate	Fly ash	Slag	PP fiber
53.9	39.9	401	160	715	883	57	115	0.7

2.2.2 Comparisons Between the Predictions and the Experimental Results

In this section, the predicted results from FE analyses are compared with the experimental results for validating the modeling method. In the experimental results, displacements are measured from the surface unexposed to fire. Then, the experimental results of load–displacement relationships of the fire-damaged walls are compared with the analytical results, as shown in Fig. 8a–d. In general, good agreement between the experiments and analyses is obtained. In particular, the maximum loads predicted from the FE analyses match well with the experimental results, and both FE and experimental results show that the maximum load

decreases as the heated area increases. Mismatches between the FE predictions and experiments are mostly caused by the asymmetric wall behavior observed from the experiments, such that there is relatively large difference between the displacements of analyses and test results while maximum load shows great agreement. Compared to the experimental results, the predicted maximum displacements from the FE models of the walls heated only on half- (54S_1H) and single-surface (54S_1F) are smaller. The discrepancy between the experimental data and predictions can be explained from the experimental instrumentation and modeling approach. During the experiments, displacements of the walls were measured from the bolts inserted to

Chun *et al. Int J Concr Struct Mater*   (2022) 16:32
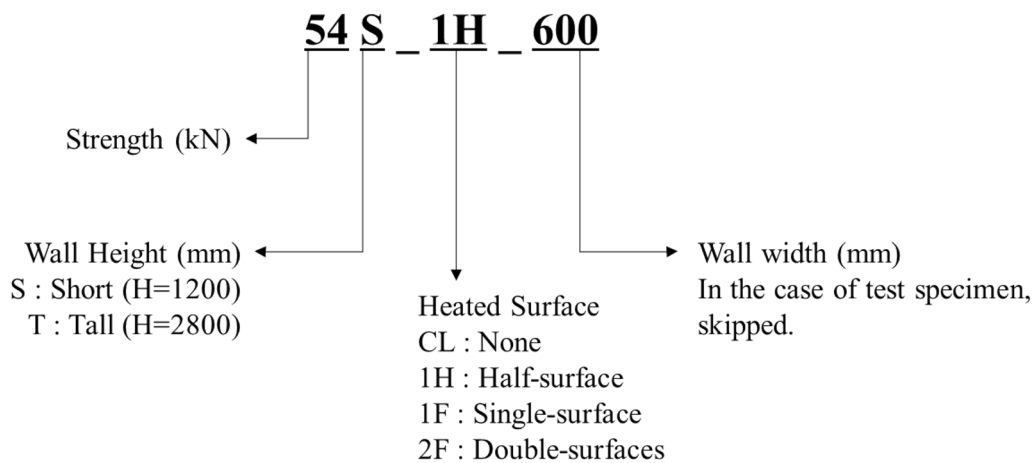
Page 7 of 14

(a) Set up for fire test   (b) ISO-834 standard heating curve   (c) Set up for loading test

Fig. 6 Experimental setup and ISO-834 standard heating curve.

Fig. 7 Terminology of specimen name.

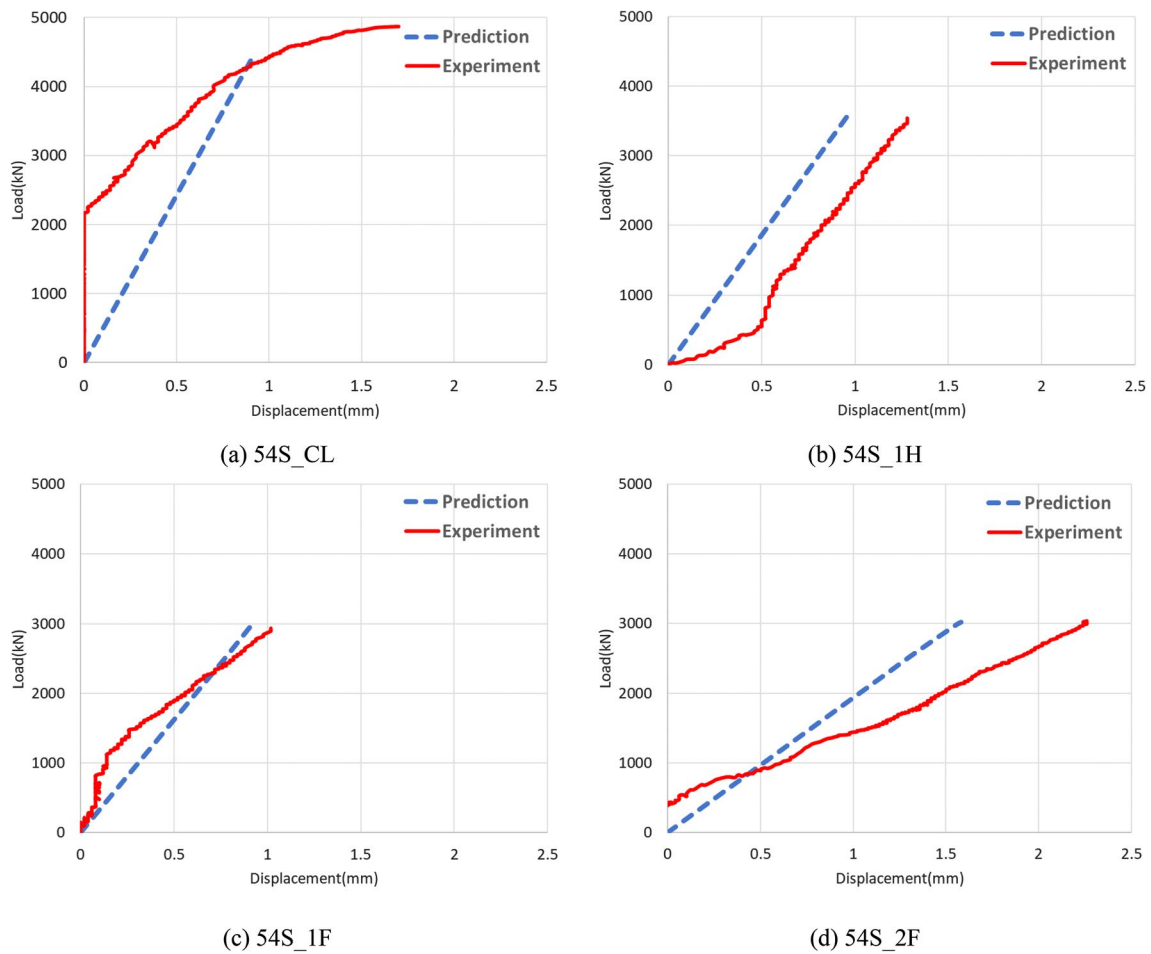**Table 5** Temperature distribution inside the walls (unit: °C).

Distance from the heated surface Specimen	20 mm	40 mm	100 mm
54S_1H	418.7	394.6	117.2
54S_1F	820.8	594.8	167.2
54S_2F	783.9	470.9	246.7

Table 6 Results of loading test.

Specimen	Heated area	Axial strength (kN)	Reduction ratio of axial strength to control specimen (%)
54S_CL	None	4870.3	0
54S_1H	Half-surface	3918.6	19.54
54S_1F	Single-surface	3195.0	34.40
54S_2F	Double-surfaces	3041.7	37.55

both front and back surfaces of the walls. However, bolts on the surface exposed to fire were slipped during the loading due to the damaged wall surfaces and lead to overestimation of displacement. Once excluding the experimental data measured from the damaged wall surfaces, and comparing predictions with the

experimental results obtained only from the undamaged wall surfaces as shown in Fig. 8, the predictions are in better agreements with the experimental data. One may point out that the maximum displacements are still larger in the experiment than in the prediction.

Fig. 8 Load–displacement curves obtained from FE analysis and experiments.

Table 7 Results of axial strength.

Specimen	Heated area	Experiment	FE analysis	Ratio between the experimental and analytical results
		Maximum axial strength (a) (kN)	Maximum axial strength (b) (kN)	(b)/(a)
54S_CL	None	4870.3	4436.0	0.911
54S_1H	Half-surface	3918.6	3557.3	0.907
54S_1F	Single-surface	3195.0	3052.8	0.955
54S_2F	Double-surfaces	3041.7	3023.0	0.994

This is because the material model did not include concrete shear. Nonetheless, the displacement difference is as minimal as less than 1 mm in magnitude while the maximum loads are well matched between the experiments and the predictions. When the walls are partially exposed to fire, the top head of the wall tends to be tilted, thus mismatch between the loading panel and top head of the wall may cause slip in the early stage of loading. Despite the discrepancy of maximum displacement between the experiment and the model, the predicted results clearly show the decrease of maximum load with increase of heated area, and the ratios of the predicted results to the experiments are close to 1, as shown in Table 7. Therefore, it can be said that the FE

Chun *et al. Int J Concr Struct Mater*   (2022) 16:32

Page 9 of 14

models are able to capture the structural behavior of fire-damaged walls affected by the heated area.

3 Parametric Study

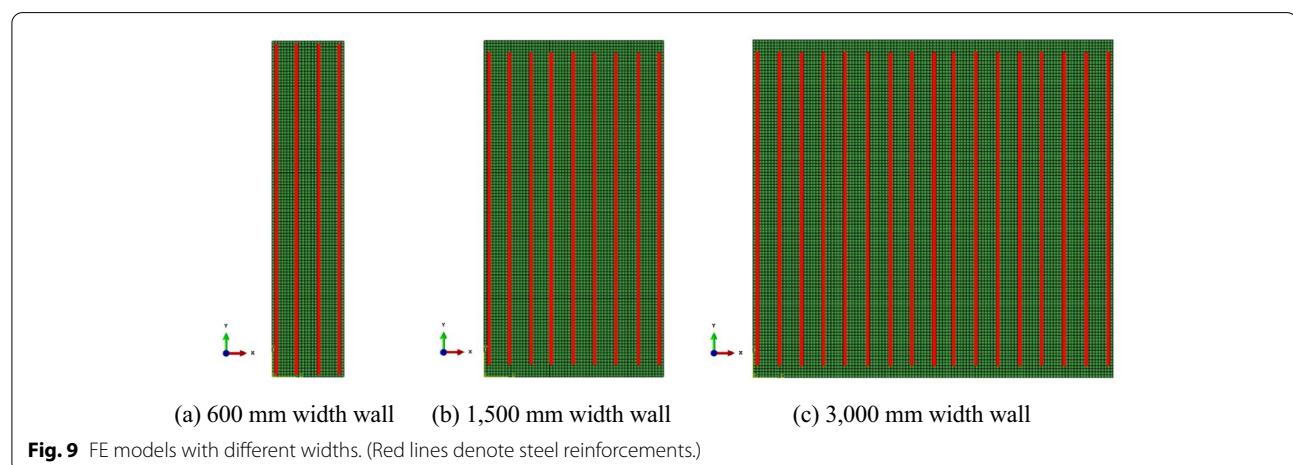### 3.1 Axial Strength of Fire-Damaged Walls in Real-scale

Using the analytical approaches validated in Sect. 2.2, the more analytical studies are conducted for the axial strength of fire-damaged walls in real scale. The walls are of various widths of 600, 1,500, and 3,000 mm, as illustrated in Fig. 9a–c, and the heated areas are varied as half-surface, single-surface and double-surfaces. The wall height is fixed as 2,800 mm, and constant thickness of 200 mm is used for all cases which makes slenderness values are controlled to be same as 45.029. These dimensions are determined based on the sizes of the walls in typical residential buildings in Korea. In addition, vertical reinforcements are included in the model to have ratio and intervals similar to those of the short walls used for the validation. Details of the model names, dimensions, heated areas and steel reinforcements are listed in Table 8. Pin support conditions are prescribed to the upper and lower part of the walls as if the walls are constrained by the slabs having 100 mm of thickness. Thus, nodes on the part from the bottom surface to 100 mm of height are restrained in all translational directions, and the nodes on the part from the top surface to 2700 mm of height are restrained in horizontal directions. Loading is applied to the top surface of the wall models in the form of displacement control. The temperature distributions inside the walls and the material contents are assumed as same to those of small sized wall models generated for the validation. Thus, nonlinear and temperature-dependent material properties are also considered in the analyses for the parametric studies by assigning

Table 8 Variables of FE models for parametric studies.

FE model	Wall dimension	Heated area	Reinforcement
54T_CL_600	600 mm (width) 2,800 mm (height) 200 mm (thickness)	None	8-D10
54T_1H_600		Half-surface	
54T_1F_600		Single-surface	
54T_2F_600		Double-surfaces	
54T_CL_1500	1,500 mm (width) 2,800 mm (height) 200 mm (thickness)	None	18-D10
54T_1H_1500		Half-surface	
54T_1F_1500		Single-surface	
54T_2F_1500		Double-surfaces	
54T_CL_3000	3,000 mm (width) 2,800 mm (height) 200 mm (thickness)	None	34-D10
54T_1H_3000		Half-surface	
54T_1F_3000		Single-surface	
54T_2F_3000		Double-surfaces	

material properties of different temperatures to the corresponding part of the concrete and steel.

Table 9 lists the predicted results of wall models having different wall widths and heated areas. It is common that the greater the heated area, the more the axial strength decreases, regardless of the wall width. In order to fairly compare the axial strengths of the walls having different widths and heated areas, the strength reduction ratios for the heated wall models are calculated using Eq. (1), and found to be 7–16, 35–41, and 56–57% for the walls heated on half-surface, single-surface and double-surfaces, respectively. It is interesting to note that, for the walls in real scale, the reduction ratios of the walls heated on double-surface are much larger than that of the walls heated on single-surface as well as the short walls heated on double-surfaces. This is not observed from the short walls, maybe because the aspect ratios (ratio of height to thickness) of the walls in real scale become much larger than those of the short walls especially when heated on

(a) 600 mm width wall   (b) 1,500 mm width wall   (c) 3,000 mm width wall

Fig. 9 FE models with different widths. (Red lines denote steel reinforcements.)

Chun *et al. Int J Concr Struct Mater*   (2022) 16:32

Page 10 of 14

Table 9 Predicted results of the models with different wall widths and heated areas.

	Name	Axial strength (kN)	Strength reduction ratio to unheated model (%)
Short walls—experiments	54S_CL_600	4870.3	0
	54S_1H_600	3918.6	19.54
	54S_1F_600	3195.0	34.40
	54S_2F_600	3041.7	37.55
Tall walls—FE predictions	54T_CL_600	6774	0
	54T_1H_600	5569	17.78
	54T_1F_600	4375	35.41
	54T_2F_600	3003	55.67
	54T_CL_1500	16,087	0
	54T_1H_1500	13,541	15.83
	54T_1F_1500	9434	41.36
	54T_2F_1500	6893	57.15
	54T_CL_3000	28,325	0
	54T_1H_3000	26,278	7.23
	54T_1F_3000	17,467	38.33
	54T_2F_3000	12,435	56.10

double-surfaces and cause stability issue. Whereas, the strength reduction ratios of the half-surface heated walls in real scale are much smaller than those of the short walls, because the area of undamaged part is large enough to resist the applied load. Regarding the wall width, it seems that the axial strength reduction ratio slightly decreases with the wall width, especially when half of the wall surface is exposed to fire. However, for the walls heated on a full surface or the larger area, it is observed that the effect of wall width on the axial strength reduction ratio is minimal or even slightly increase. This may be explained from the relationship between wall width and the fire-damaged area. Wall width works for residual strength of the fire-damaged walls when only partial area of the surface is exposed to fire, because the increased undamaged part with the increased wall width resists against buckling. Whereas, the walls heated on single and double-surfaces cannot resist local buckling as much as the wall heated on half-surface does and increase of wall width does not significantly reduce axial force reduction ratios.

walls from the proposed equations are well matched with the simulation and experiments. In addition, the solid lines in the graphs show trends of how axial strength reduction ratios of the fire-damaged walls change depending on wall width and heat exposure condition. As commonly shown, the axial strength increases almost linearly with the wall width. In addition, it is found that the maximum displacement at wall failure decreases with the wall width, which tells that the more brittle behavior can be expected from the fire-damaged walls in real scale.
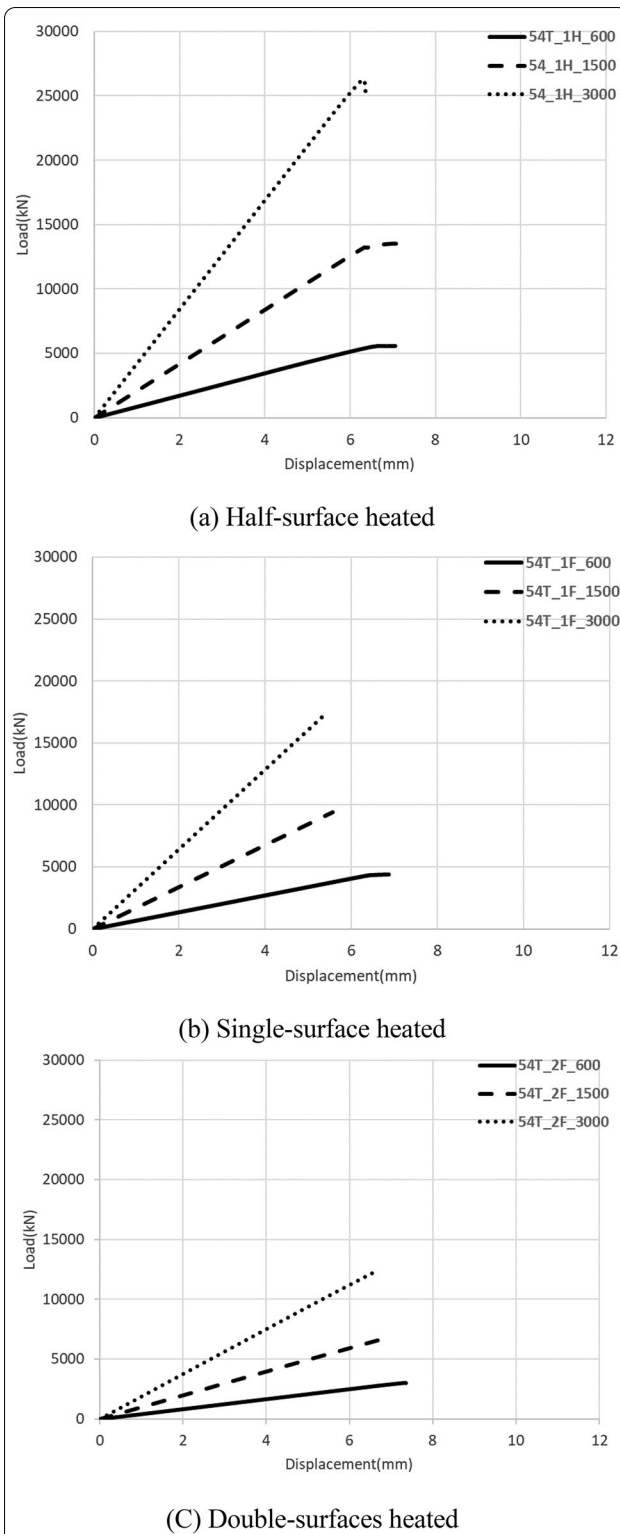
4 Discussion

In the previous chapter, the axial strengths for the fire-damaged walls with various sizes and heated areas are investigated experimentally and analytically. In this chapter, regression analyses are performed using the statistical analysis tool, R (version 3.6.1, The R Foundation for Statistical Computing, R Core Team, 2014) to express the numerical relationships between the axial strength reduction ratios of fire-damaged walls and influencing

$$\text{Axial strength reduction ratio} = \left(1 - \frac{\text{max. load} - \text{bearing capacity of heated wall model}}{\text{max. load} - \text{bearing capacity of control wall model}}\right) \times 100. \tag{1}$$

Fig. 10a–c are the load–displacement curves of the walls predicted from the analyses which shows estimation of axial strength reduction ratios of fire-damaged

factors. In addition to the results obtained from these experimental and analytical studies, available test data are collected from the previously published literature of

Fig. 10 Prediction of load–displacement of fire-damaged walls in real scale.

(a) Half-surface heated

(b) Single-surface heated

(C) Double-surfaces heated

our research group (Kang, 2017) as shown in Table 10. This data includes test variables of concrete strength, wall width and height and number of heated surfaces. The difference between the total height and effective height of the wall is due to constrained part. Thus, only the wall part in the effective height is allowed to deform during heating and loading.

In the regression analyses, the number of heated surfaces is considered as a categorical variable, because the experimental results show that the axial strength of fire-damaged wall is not linearly correlated to the number of heated surfaces. Even so, the number of heated surfaces multiplied with the wall width is additionally included in the regression analyses as a continuous variable, in order to consider the combined effect of the heated surfaces and wall width on the axial strength reduction ratios of fire-damaged walls.

From the regression analysis, multiple linear formulations are found as Eqs. (2)–(4). The linear formulations without having polynomial term are considered as accurate enough to estimate axial strength reduction ratios of the fire-damaged walls, because the multiple R^2 value is obtained as 0.93. Fig. 11a illustrates axial strengths reduction ratios for the fire-damaged walls having different wall width and number of heated surfaces, obtained from the formulations as well as the simulation/experiments. This figure shows that there is significant effect of wall width and number of heated surfaces on the axial strength reduction ratios. Also the estimated axial strength reduction ratios obtained from the formulations are similar to the simulation/experimental results. Fig. 11b also shows that the estimated axial strength reduction ratios from the formulations are well agreed with the experimental results, considering influencing parameters such as concrete strength, wall width, and number of heated surfaces:

$$P_{1h} = 1 - (-1.5e^{-3} \cdot f_c + 8.2e^{-5} \cdot l - 4.8e^{-5} \\ \cdot h - 6.08e^{-5} \cdot l \cdot n + 0.97, \tag{2}$$

$$P_{1f} = 1 - (-1.5e^{-3} \cdot f_c + 8.2e^{-5} \cdot l - 4.8e^{-5} \\ \cdot h - 0.20 \cdot n - 6.08e^{-5} \cdot l \cdot n + 0.77, \tag{3}$$

$$P_{2f} = 1 - (-1.5e^{-3} \cdot f_c + 8.2e^{-5} \cdot l - 4.8e^{-5} \\ \cdot h - 0.23 \cdot n - 6.08e^{-5} \cdot l \cdot n + 0.74, \tag{4}$$

where P = axial strength reduction ratio (1 h: half-surface heated, 1f: single-surface hated, 2f: double-surfaces heated); f_c = concrete strength (MPa); l = wall width (mm). h = wall height(mm); and n = number of heated surfaces (0.5, 1, or 2).
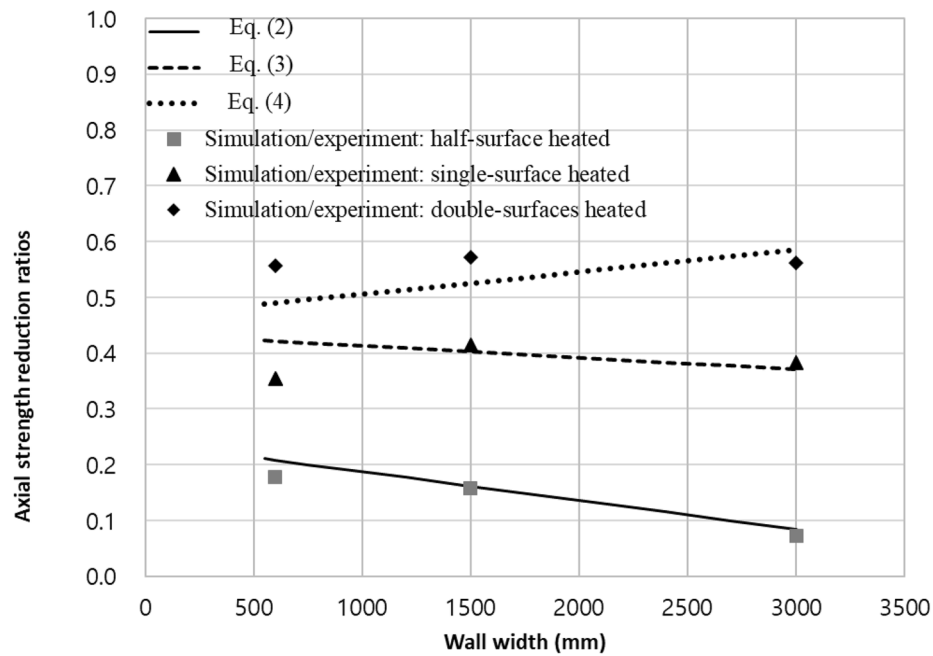
Table 10 Collected information of the fire-damaged walls for regression analysis.

Name	Concrete strength (MPa)	Width (mm)	Total height (effective height, mm)	Number of heated surfaces	Axial strength (kN)
27S_CL_750	26.8	750	1300 (600)	0	3545.0
27S_1F_750				1	2335.0
40S_CL_600	53.9	600	1200 (600)	0	4870.3
40S_1H_600				0.5	3918.6
40S_1F_600				1	3195.0
40S_2F_600				2	3041.7
54S_CL_600	41			0	4438.0
54S_1H_600				0.5	4112.0
54S_1F_600				1	3106.0
54S_2F_600				2	3007.0
54T_CL_600	53.9		2800 (2600)	0	6773.5
54T_1H_600				0.5	5569.0
54T_1F_600				1	4375.0
54T_2F_600				2	3003.0
54T_CL_1500		1500		0	16,087.0
54T_1H_1500				0.5	13,541.0
54T_1F_1500				1	9433.5
54T_2F_1500				2	6893.0
54T_CL_3000		3000		0	28,324.7
54T_1H_3000				0.5	26,278.0
54T_1F_3000				1	17,466.6
54T_2F_3000				2	12,435.0

5 Conclusions

This paper investigates the effects of wall width and fire-damaged area on the axial strength of fire-damaged RC walls using FE and statistical analysis. For validation of the analytical method, axial loading test results are used for the walls heated on half-, single-, and double-surfaces. Once the FE modeling method is validated by comparison with the experimental results, the parametric studies are performed to cover the fire-damaged wall models with the longer and the higher dimensions in real scale. Finally, the experimental and analytical results together with the collected data from the previously published literature of our research group are used to perform regression analyses. The conclusions of this study are as follows:

(1) The analytical methods using temperature-dependent material properties of concrete and steel reinforcements and experimental results of temperature distribution inside the walls are validated with experimental results of load–displacement curves of fire-damaged short walls. Both predicted and experimental results show maximum loads decrease with increasing of heated area.

(2) The analytical studies of the fire-damaged walls in real scale show that the reduction ratio of axial strength decreases as the wall width increases, especially when the heated area is relatively small as half of the surface. However, for the walls heated on single or double-surfaces, axial strength reduction ratio is similar or even slightly increases with the wall width.

(3) From the regression analysis, first-order formulations to estimate axial strength reduction ratios of the fire-damaged concrete walls are obtained. From the comparisons with analytical and experimental results, it is found that the formulations are able to estimate axial strength reduction ratios of the fire-damaged concrete walls considering the various influencing parameters of the wall size, concrete strength and fire-damaged area. However, the suggested formulations are limited to the concrete walls having 28-day compressive strengths of 26.8–53.9 MPa, heated according to the ISO-834 time temperature curves, and width of 600-3000 mm. Further research can be suggested to expand the formulations for the application toward other types

Chun *et al. Int J Concr Struct Mater* (2022) 16:32

Page 13 of 14

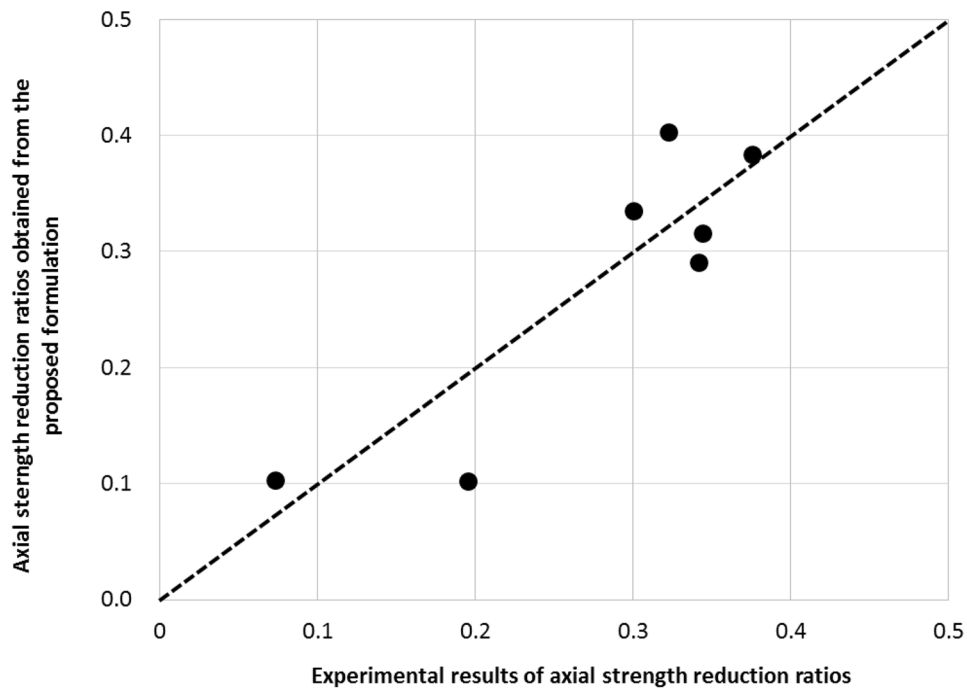P = axial strength reduction ratio

 (1h: half-surface heated, 1f: single-surface heated, 2f: double-surfaces heated)

fc = concrete strength(MPa), l=wall length(mm), h=wall height(mm)

n = number of heated surfaces (0.5, 1, or 2)

(a) Axial strength of fire-damaged walls having different widths and heated surfaces

(b) Axial strength of fire-damaged walls

Fig. 11 Results from regression analyses with comparison of experimental and analytical data.

Chun *et al. Int J Concr Struct Mater*   (2022) 16:32

Page 14 of 14

of structural members and establish a comprehensive database of structural performance of fire-damaged structures.

Authors' information
Y. Chun is a Ph.D candidate from Department of Architectural and Urban Systems Engineering, Ewha Womans University, 52, Ewhayeodae-gil, Seodaemun-gu, Seoul, Republic of Korea under preparation of a Ph.D. dissertation, which topic is adopting concrete design to other research area.
E. Ryu is a researcher of Dept. of Fire safety research, Korea Institute of Civil Engineering and Building Technology, 64, 182Beon-Gil, Mado-Ro, Mado-Myeon, Hwaseong-Si, Gyeonggi-do, Republic of Korea,. Her major research area is fire in building.
Y. Lee is a researcher of Dept. of Construction Industry Promotion, Korea Institute of Civil Engineering and Building Technology, 283, Goyang-daero, Ilsanseo-gu, Goyang-si, Gyeonggi-do, Republic of Korea,. Her current research area is making code and standard in building in Korea.
H. Kim is a professor in Department of Architectural and Urban Systems Engineering, Ewha Womans University, 52, Ewhayeodae-gil, Seodaemun-gu, Seoul, Republic of Korea. She has studied analytical methods to predict structural performance of fire-damaged concrete structures and bio-composite.
Y. Shin is a professor in Department of Architectural and Urban Systems Engineering, Ewha Womans University, 52, Ewhayeodae-gil, Seodaemun-gu, Seoul, Republic of Korea. His major research areas are design and safety evaluation of concrete structures and materials associated with fire and earthquake.

Availability of data and materials
The data and materials had been included in the manuscript.

Declarations

Competing interests
The authors declare that they have no competing interests.

References
ABAQUS. (2010). *Theory manual version 6.10-3*. Dassault Systems Simulia Corp.
ACI, TMS Committee 216. (1989). *Guide for determining the fire endurance of concrete elements (ACI 216R–89), Reapproved 2001*. American Concrete Institute.
AS 3600. (2001). *Concrete structures*. Standards Association of Australia.
Cheng, F., Kodur, V., & Wang, T. (2004). Stress-strain curves for high strength concrete at elevated temperature. *Journal of Materials in Civil Engineering, 16*(1), 84–90.
Chun Y, Lee Y, Kim H, Shin Y (2018) Effect of Mixture Ratios on Thermal Behaviors of High Strength Concrete Walls Exposed to Fire on Foreside. IOP Conference Ser.: Material Science Engineering 431, 042010
Chun Y (2019) A study on the residual strength of RC walls exposed to fire, Master's dissertation, Ewha Womans University.
Eurocode 2. (2004). *Design of concrete structures. Part 1–2: General rules-structural fire design prEN1992-1-2*. European Standard.
Kang J (2017) Performance assessment of reinforced concrete bearing wall subjected to fire. Ph.D dissertation, Ewha Womans University
Kang, J., Yoon, H., Kim, W., Kodur, V., Shin, Y., & Kim, H. (2016). Effect of wall thickness on thermal behaviors of RC walls under fire conditions. *International Journal of Concrete Structures and Materials, 10*(3), 19–31.
Kang, J., Yoon, H., Ryu, E., & Shin, Y. (2019). Analytical studies for the effect of thickness and axial load on load bearing capacity of fire damaged concrete walls with different sizes. *Journal of Structural Integrity and Maintenance, 4*(2), 58–64.
KCS 14 20 33: 2020, Korean construction standard center: Design standard for high strength concrete, p. 2 (In Korean)
Kodur V, Sultan M (1998) Structural behaviour of high strength concrete columns exposed to fire. International Symposium on High Performance and Reactive Powder Concrete 217–232
Lee, S., & Lee, C. (2013). Fire resistance of reinforced concrete bearing walls subjected to all-sided fire exposure. *Materials and Structures., 46*(6), 943–957.
Liu, G., Song, Y., & Qu, F. (2010). Post-fire cyclic behavior of reinforced concrete shear walls. *Journal of Central South University of Technology, 17*(5), 1103–1108.
Ngo, T., Fragomeni, S., Mendis, P., & Ta, B. (2013). Testing of normal- and high-strength walls subjected to both standard and hydrocarbon fires. *ACI Structural Journal, 110*(3), 503–510.
Nguyen, K., Ngo, T., Mendis, P., & Heath, D. (2018). Performance of high-strength concrete walls exposed to fire. *Advances in Structural Engineering, 21*(8), 1173–1182.
Ni, S., & Bairely, A. C. (2018). Simulation procedure for the post-fire seismic analysis of reinforced concrete structural walls. *Fire Safety Journal, 95*, 101–112.
NZS 3101. (1995). *Concrete structures standard. Part 1—The design of concrete structures*. New Zealand Standards.
O'Meagher, A. J., & Bennetts, I. D. (1991). Modeling of concrete walls in fire. *Fire Safety Journal, 17*, 315–335.
Otmani-Benmehidi, N., Arar, M., & Chine, I. (2014). Modeling the behavior of reinforced concrete walls under fire, considering the impact of the span on firewalls. *The International Journal of Soft Computing and Software Engineering, 3*(3), 600–607.
Poon, C., Azhar, S., Anson, M., & Wong, Y. (2001). Strength and durability recovery of fire-damaged concrete after post-fire-curing. *Cement and Concrete Research, 31*, 1307–1318.
Poon, C., Azhar, S., & Wong, Y. (2016). *Concrete under fire: Damage mechanisms and residual properties*. The Hong Kong Polytechnic University.
R Core Team (2014) R: A language and environment for statistical computing. R Foundation for Statistical Computing, Vienna, Austria. http://www.R-project.org/
Ryu, E., Kim, H., Chun, Y., Yeo, I., & Shin, Y. (2020). Effect of heated areas on thermal response and structural behavior of reinforced concrete walls exposed to fire. *Engineering Structures*. https://doi.org/10.1016/j.engstruct.2020.110165

Publisher's Note
Springer Nature remains neutral with regard to jurisdictional claims in published maps and institutional affiliations.